Int. J. Heat Mass Transfer. Vol. 35, No. 5, pp. 1247–1260, 1992
Printed in Great Britain

0017–9310/92 $5.00 + 0.00

Critical heat flux enhancement by means of liquid subcooling and centrifugal force induced by flow curvature

JESSE E. GALLOWAY and ISSAM MUDAWAR

Boiling and Two-Phase Flow Laboratory, School of Mechanical Engineering,
Purdue University, West Laffayette, IN 47907, U.S.A.

(*Received* 15 *February* 1991 *and in final form* 1 *May* 1991)

Abstract—Experiments are performed to assess the feasibility of cooling high flux heat sources flush mounted on the inner wall of a cylindrical vessel by a dielectric liquid flowing at high velocity parallel to the vessel wall. Fluid motion is induced by rotating a stirrer having radial blades about the axis of the vessel. The study focusses on examining critical heat flux (CHF) enhancement attributed to liquid subcooling and the centrifugal body force induced by fluid rotation. This includes using test vessels with different inner radii, 4.19 and 7.62 cm, three heater lengths, 1.27, 2.54 and 5.08 cm, and stirrers having two or four blades. CHF is found to be independent of heater length and the number of stirrer blades. CHF enhancement is achieved by increasing the liquid fill volume, increasing the rotational speed and/or decreasing the radius of curvature. The system facilitates the removal of heat at nearly isothermal wall conditions over a wide range of heat fluxes. A CHF correlation is presented which accounts for the effects of subcooling and centrifugal force over all conditions tested.

1. INTRODUCTION

MORE AGGRESSIVE cooling techniques will be required in the near future to cool high flux devices such as laser mirrors, X-ray tubes, and high power electronic chips. For example, chip heat fluxes in excess of 100 W cm^{-2} have already been projected for the mid-1990s [1], while reliability constraints would still require the chip temperature to be maintained below approximately 85°C [2]. Many researchers have proposed boiling heat transfer as an attractive cooling mode capable of meeting the projected heat fluxes. Relatively large heat flux levels are possible during nucleate boiling while simultaneously maintaining a low surface temperature. However, an upper heat flux limit exists for nucleate boiling, commonly called the critical heat flux (CHF). Beyond CHF, liquid contact with the boiling surface is inhibited due to the formation of a thermally-insulating vapor blanket adjacent to the surface. A sudden rise in surface temperature follows, which most likely would result in permanent damage to the device. Because of the nature of this catastrophic failure, an understanding of CHF is of great practical importance.

CHF can be enhanced in order to extend the useful range of heat flux attainable in the nucleate boiling regime. One enhancement method is to increase the body force normal to the boiling surface, thereby aiding in vapor removal from the surface during vigorous boiling. A large body force can be created normal to the boiling surface if, for example, the surface is mounted on the inner wall of a cylindrical vessel filled with liquid and rotated about its axis. This approach was successful in enhancing CHF as demonstrated experimentally by Merte and Clark [3] and Marto and Gray [4]. Usenko and Fainzil'berg [5] and Costello and Adams [6] reported that CHF increased with acceleration following the classical CHF relation proposed by Zuber *et al.* [7], $q_m \propto (a/g)^{1/4}$, where $a = \omega^2 R$. Costello and Tuthill [8] and Beckman and Merte [9] reported that the bubble departure frequency increased with acceleration while the bubble departure diameter decreased, thus reducing vapor layer obstruction near the heater surface. Therefore, more efficient vapor removal is possible at higher rotational speeds, which increases CHF.

A more practical means for increasing the body force normal to the heater surface is desired, that would avoid the difficulties encountered in making electronic connections to a rotating system. Mudawar (see ref. [10]) proposed enhancing CHF by mounting heat sources on a curved surface over which a coolant is supplied at a high velocity, taking advantage of the centrifugal force created normal to the surface of the heat source. Carver *et al.* [11], Miropol'skiy and Pikus [12], and Gu *et al.* [13] experimentally verified CHF enhancement due to stream-wise curvature of the heated surface. Gambill and Green [14] induced swirl flow inside a heated tube using a vortex inlet and measured a greater than 200% increase in CHF compared to linear flow. Dhir and Scott [15], using a similar arrangement, measured up to 80% enhancement compared to flow in a straight tube. The findings from these studies reveal that surface curvature enhances boiling heat transfer by centrifuging vapor away from the boiling surface.

Another means for enhancing CHF is to subcool the liquid below its saturation temperature. Sub-

NOMENCLATURE

a	external body force
C	propagation speed of interfacial perturbation
c	constant in equation (2)
c_{pf}	specific heat of liquid at constant pressure
g	acceleration due to gravity
h_{fg}	latent heat of vaporization
L	heater length
N	number of stirrer blades
P_{core}	pressure measured in the vapor core
P_{sat}	saturation pressure
P_w	pressure at test vessel wall
ΔP	pressure rise across liquid layer, $P_w - P_{core}$
q	heat flux (electric power input divided by chip surface area)
q_m	critical heat flux (CHF)
q_m^*	dimensionless CHF, defined in Fig. 12
R	inner radius of test vessel
R_c	transitional radius, defined by equations (1) and (2)
r	radial coordinate
T_w	mean surface temperature
T_{sat}	saturation temperature
ΔT_{sat}	$T_w - T_{sat}$
t	thickness of liquid layer; time
U_c	characteristic velocity in an agitated vessel, predicted by equation (2) for $r = R$
U_m	mean flow velocity
U_s	stirrer tip velocity, $(R-\delta)\omega$
V	fill volume
V_{cl}	clearance volume
x	spatial coordinate
z	coordinate defining position of perturbed interface
z_0	amplitude of interfacial perturbation.

Greek symbols

δ	stirrer tip clearance
λ	wavelength of interfacial perturbation
λ_c	wavelength corresponding to onset of interfacial instability
λ_d	wavelength corresponding to fastest ('most dangerous') growth of interfacial instability
ρ_f	density of saturated liquid
ρ_g	density of saturated vapor
σ	surface tension
ω	rotational speed.

Subscripts

f	saturated liquid
g	saturated vapor
H	Helmholtz
sat	saturated
sub	subcooled
T	Taylor.

cooling increases bubble condensation and reduces vapor accumulation near the heater surface. In extremely high subcooling cases, Collier [16] reported that growing vapor embryos may condense and collapse while still attached to the heater surface. It is generally accepted that CHF increases with subcooling, ΔT_{sub} [17]. Vliet and Leppert [18] reported a linear CHF dependence on subcooling for convective boiling in cross-flow over cylinders. Katto and Ishii [19] showed that CHF is proportional to ΔT_{sub}^2 for a free jet flowing parallel to a horizontal surface. Mudawar *et al.* [20] and Mudawar and Maddox [21] also reported CHF enhancement with subcooling for the configurations of a falling film and linear channel flow, respectively.

The experimental apparatus used in the present study (Fig. 1) enhances CHF by means of centrifugal force and subcooling. A flat bladed stirrer rotating at high speed moves liquid in a stream-wise direction over the inner vessel wall. Clearly the liquid velocity directly at the heater surface must be zero due to the no-slip condition and, therefore, a centrifugal force is not experienced at the surface. However, as the bubbles emerge and are released from nucleating cavities, they penetrate into the bulk flow where radial buoyancy forces take effect. Vapor accumulation and associated pressurization within the liquid are avoided since the free liquid interface allows for 'breathing' of the vapor radially through the liquid layer. Subcooling of the liquid is achieved by the radial pressure rise across the liquid layer. Subcooling increases with increases in rotational speed and/or thickness of the liquid layer.

The purpose of this study is to quantify the dependence of CHF on the centrifugal force, liquid layer agitation, heater length and liquid subcooling. Data presented previously by Galloway and Mudawar have already demonstrated that stream-wise curvature enhances CHF. However, only a single vessel radius, single stirrer design and single heater length were tested in that study, precluding a definitive assessment of whether CHF enhancement is an outcome of surface curvature and mechanical agitation or simply a result of a greater liquid stream-wise velocity. The experimental apparatus used by Galloway and Mudawar [22] was modified to isolate the individual effects most likely to influence CHF.

In the present study, two different vessels were tested ($R = 7.62$ cm and 4.19 cm) to provide conclusive evidence whether stream-wise curvature is an

important parameter affecting CHF independent of the stream-wise velocity. A two-bladed ($N = 2$) and a four-bladed ($N = 4$) stirrer were tested in both vessels to resolve the CHF enhancement potential from liquid film agitation. This study also examined the effects of varying rotational speed, ω, liquid film thickness, t, and heater length, L.

2. EXPERIMENTAL FACILITY AND TEST PROCEDURE

The present experiments were performed with the 3M dielectric fluid FC-72 having a boiling point of 57°C at atmospheric pressure. The original experimental facility reported by Galloway and Mudawar (Fig. 1) was fabricated from G-10, a high strength fiberglass plastic having a low thermal conductivity, a feature essential for minimizing heat loses. Heat losses were also reduced by band heaters which covered the vessel exterior. A one horsepower d.c. motor was used to drive the shaft at speeds ranging from 500 to 1800 r.p.m. The saturation pressure was controlled automatically by a solenoid control valve which modulated the water flow rate through the condenser coil in response to the pressure fluctuations. Vapor generated from the boiling surface was released from the test section into the condenser region where it condensed and dripped back into the test section through the liquid feed holes. Thermocouple probes were mounted in the center of the test vessel to monitor the vapor core temperature. The saturated liquid temperature was measured by two thermocouples mounted through the heater flange protruding 0.5 mm into the liquid layer. A pressure transducer measured the vapor core pressure and a second transducer monitored the wall pressure just downstream of the heater.

A 1.27 cm × 1.27 cm heater shown in Fig. 1(b) was flush mounted to the inner surface of the 7.62 vessel. A 92 Ω thick film resistor, acting as the heating element, was silver soldered directly to the back side of the oxygen-free copper heater block.

A second vessel with a smaller radius ($R = 4.19$ cm) was designed to fit inside the original vessel, which allowed testing of a smaller boiling surface radius of

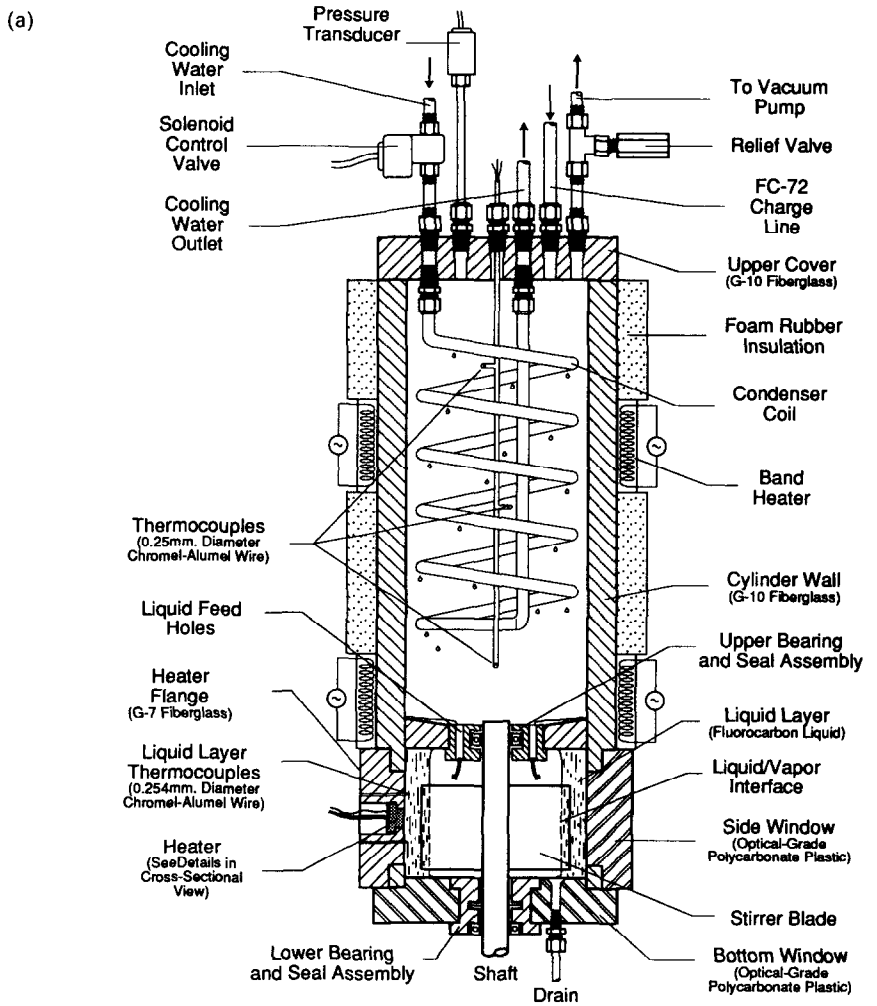

FIG. 1. Experimental test facility. (a) Longitudinal view. (b) Cross-sectional view.

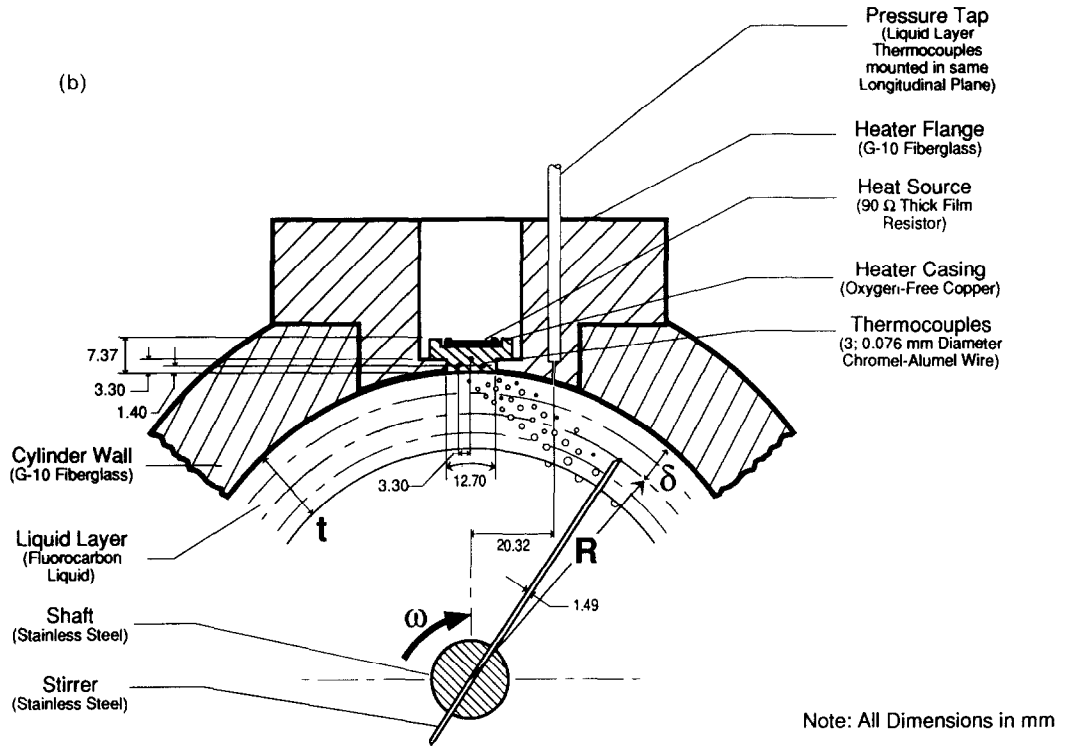

FIG. 1.—*continued.*

curvature. Three different heater lengths ($L = 1.27$, 2.54 and 5.08 cm) were tested in this smaller vessel, as shown in Fig. 2. The heaters were fabricated by silver-soldering thick film resistors to the back side of the oxygen-free copper heater blocks. The 1.27 cm heater was heated by a single thick film resistor, the 2.54 cm heater was heated by two thick film resistors wired in parallel and the 5.08 cm heater was heated by three

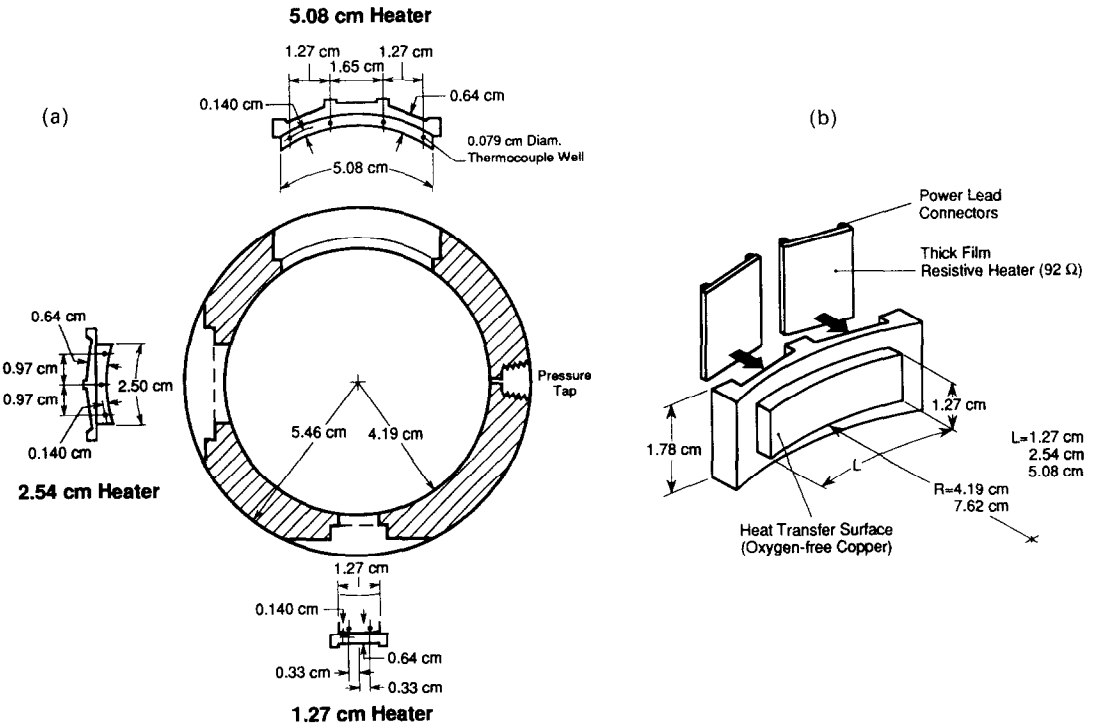

FIG. 2. Smaller test vessel ($R = 4.19$ cm). (a) Cross-sectional view. (b) Heater construction details.

thick film resistors also wired in parallel. Particular attention was given during the design of the heaters to ensure a uniform surface heat flux regardless of the heater length by trimming the resistances of individual resistors to provide equal power. Power was supplied by a 240 V variac and measured with an accuracy better than 0.5% using direct measurements from a single voltage transducer and up to three current transducers. Surface temperature was predicted from the thermocouple temperature measurements assuming one-dimensional heat conduction normal to the boiling surface with an error less than 0.2°C.

A heat conduction analysis was performed to establish an upper bound on the conjugate losses between the heater and the surrounding flange, assuming zero contact resistance between the solid mating surfaces. For a representative case with $\omega = 800$ r.p.m., $R = 7.62$ cm and $L = 1.27$ cm, the analysis predicted a maximum heat loss of 6% in the single-phase regime, 4% in the nucleate boiling regime and 5% just prior to CHF. These predictions are conservative since contact resistances greatly reduce heat loss. Because of the relatively low conjugate heat losses, the heat fluxes reported in this study were calculated by dividing the electrical power input by the boiling surface area.

A two-bladed stirrer and a four-bladed stirrer were tested in both vessels. The two-bladed stirrer was fabricated from a single 0.15 cm thick stainless steel plate which was passed through a slot in the stirrer shaft and bolted to the shaft. The four-bladed stirrer was constructed from individual blades silver-soldered to a stainless steel hub which slid over the stirrer shaft and was bolted in place. The stirrer tip clearance δ from the vessel wall was fixed at 0.64 cm during all the reported tests.

A deaeration procedure removed most of the air dissolved in the liquid using the facility shown in Fig. 3. A vacuum pump purged the non-condensible gases from the vessel, and from a graduated cylinder located above the vessel, to an absolute pressure less than 0.07 bar. Liquid deaerated in an external deaeration tank was first charged into the graduated cylinder to measure the desired liquid fill volume. A valve connecting the graduated cylinder to the test vessel was then opened to drain the liquid into the vessel. If necessary, a second deaeration was performed within the test vessel using the system reflux condenser.

The fill volume was defined as a percentage of a reference volume which was taken as the sum of the stirrer tip clearance volume, V_{cl}, and the volume occupied below the stirrer blade. The clearance volumes for the 7.62 cm and 4.19 cm radii vessels are 360 ml and 170 ml, respectively. An additional amount of liquid was introduced to account for the mass of vapor occupying the condenser region.

A systematic procedure was imposed during all the

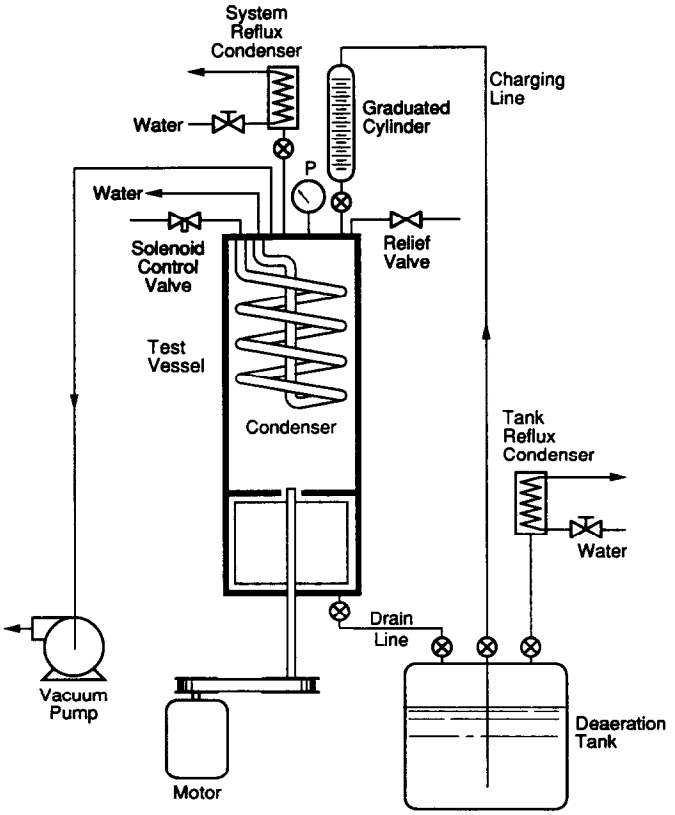

FIG. 3. Deaeration, purging and charging components.

tests to prevent contamination of the test fluid or surface aging and to ensure repeatability in the data base. Before each test, the boiling surface was blasted with a water/air/silica slurry to remove any surface residue and to produce a well-characterized surface micro-structure. Afterwards, the surface was wiped clean with a cotton cloth wetted in methanol. The surface roughness was determined with a scanning electron microscope which measured an average cavity size of the order of 10 μm.

The operating procedure consisted of: (1) deaerating the fluid by vigorous boiling and reflux condensation for a period of no less than 20 min; (2) evacuating the test vessel and associated plumbing; (3) charging the fluid into the test vessel; (4) measuring CHF for a reference condition making sure measurements were in agreement with a reference value within a band of ± 2.5 W cm^{-2}; (5) obtaining CHF data for other conditions of interest; (6) measuring CHF for the reference condition periodically and before a series of tests was completed. The tests were halted any time CHF increased due to surface aging effects by more than 2.0 W cm^{-2} above the first recorded CHF value measured at the reference condition. This happened approximately 15% of the time and those data points were discarded.

3. RESULTS AND DISCUSSION

Experimental measurements were taken to quantify the effects of CHF enhancement due to the centrifugal force and subcooling. The full boiling curves shown in Fig. 4 demonstrate the unique and nearly ideal nucleate boiling performance attainable with the present system as a result of the combined enhancement

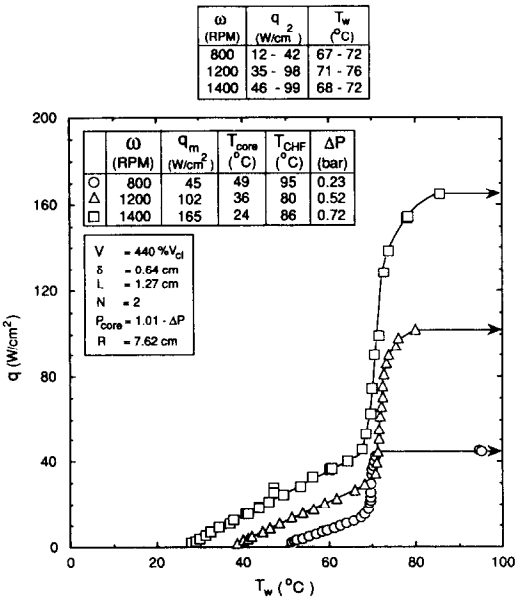

FIG. 4. Example of the nearly isothermal nucleate boiling heat transfer performance attainable with the present system.

effects attributed to subcooling and centrifugal force. A fill volume of 440% V_{cl} provides the greatest subcooling possible for the present system. At a rotational speed of 1400 r.p.m., the heater surface temperature increased by less than 4°C for a 53 W cm^{-2} increase in heat flux, a nearly isothermal performance associated with extremely high heat transfer coefficients prevailing over a wide range of heat fluxes.

Fill volume effect

Fill volumes smaller than 100% exhibited significant churning of the liquid layer, as viewed through the side window with the aid of a stroboscope, even in the absence of boiling. The interface becomes quite stable with a fill volume equal to, or greater than, 100% V_{cl}.

For fill volumes less than 100% V_{cl}, CHF was accompanied by relatively large surface temperature oscillations because of insufficient wetting at the heater surface. There could be small time intervals between successive passes of the stirrer where the heater surface was dry, even when power was not being supplied to the heater.

The heater design shown in Fig. 1(b) was modified for transient surface temperature measurements in the 7.62 cm radius vessel. A micro-thermocouple having a bead diameter of 0.076 mm was flush mounted with thermally insulating epoxy in a 0.76 mm by 0.38 mm groove milled into the heater surface. This construction allowed the thermocouple to respond more to the two-phase flow over the heater surface than to conditions in the heater block. Transient surface temperatures were measured as shown in Fig. 5 for conditions at 95% CHF, $\omega = 500$ r.p.m., and fill volumes equal to 50%, 100% and 400% V_{cl}. Large temperature oscillations were measured at a fill volume equal to 50% V_{cl}. As the heater power was increased, the dryout periods became longer and/or more frequent due to the vigorous vapor production limiting liquid contact with the heater surface. Although intermittent wetting by the stirrer blades seemed to provide some cooling at these high flux conditions, a condition was finally reached where the sweeping motion could no longer wet the surface to sustain periods of stable nucleate boiling. As the fill volume increases so does the liquid layer thickness and the radial pressure acting on the heater surface. This tends to thrust liquid towards the heater surface and enhance CHF by promoting greater liquid contact with the surface.

Subcooling effects

Subcooling results any time the liquid temperature is lowered below its saturation temperature corresponding to the local pressure. Subcooling in the present study resulted from an increase in pressure at the vessel wall with a corresponding rise in saturated temperature while the liquid temperature remained essentially in equilibrium with the saturated vapor core. Temperature measurements taken by the liquid layer thermocouples closely agreed with the tem-

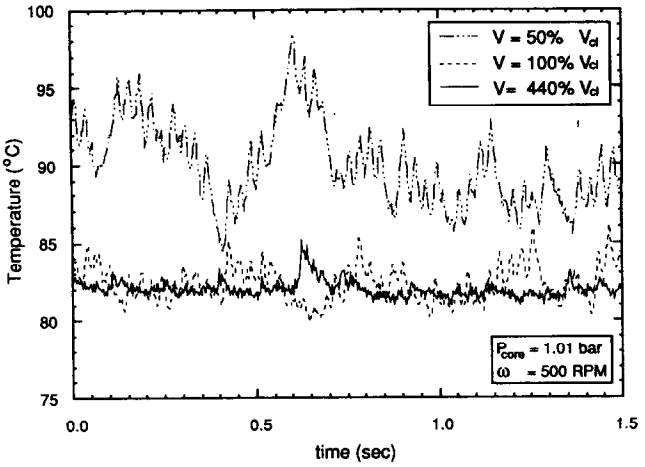

FIG. 5. Transient surface temperature measured at 95% CHF for different fill volumes.

peratures measured by the vapor core temperature probe over the full range of fill volumes and rotational speeds. The thermodynamic states of the vapor core and liquid layer are summarized in Fig. 6.

The effects of subcooling were studied for the case of $R = 7.62$ cm and fill volume equal to 440% V_{cl}. Figure 6 shows a significant change of slope in the variation of CHF with stirrer tip velocity for velocities exceeding 7.0 m s^{-1}. However, no such significant change in slope was observed for fill volumes equal to 50% and 100% V_{cl}. At first it was believed that the increase in slope was largely a result of the greater pressure at the surface of the heater. It is a well known fact that CHF increases with increasing pressure and that greater film thicknesses and higher rotational speeds both tend to increase the pressure at the wall. To isolate the effect of pressure on CHF, experiments were performed with a constant pressure at the vessel inner wall, $P_w = 1.01$ bar, by reducing the saturation pressure in the vapor core to offset the pressure rise through the liquid film as the rotational speed was incremently increased. Instead of reducing CHF, the lower wall pressure data exhibited a steeper slope with velocity, as clearly shown in Case 2 of Fig. 6.

This behavior may be understood more fully by plotting the pressure–temperature saturation curve for FC-72 along with the measured wall and saturated vapor core pressures as a function of the measured liquid and saturated vapor temperatures. Figure 7 illustrates the two cases considered. Case 1 corresponds to a constant core pressure of 1.01 bar, while Case 2 is for a constant wall pressure of 1.01 bar. Both cases have an approximately equal pressure rise in the liquid layer for equal stirrer tip velocities. The amount of subcooling for Case 2 is higher than for Case 1 due to the increasing slope of the pressure–temperature saturation curve of the coolant with increasing pressure. At $\Delta P = 0.72$ bar, Case 2 produces a subcooling at the wall almost twice that of Case 1, resulting in

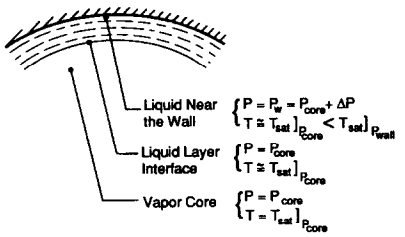

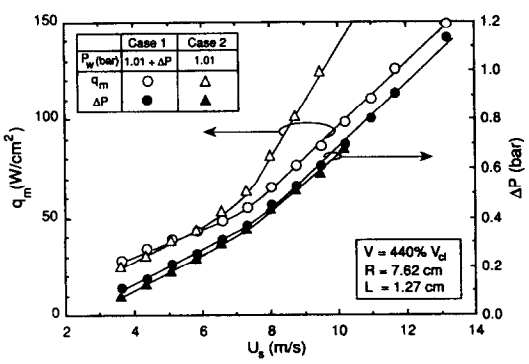

FIG. 6. Effect of stirrer tip velocity on pressure rise across liquid layer and on CHF.

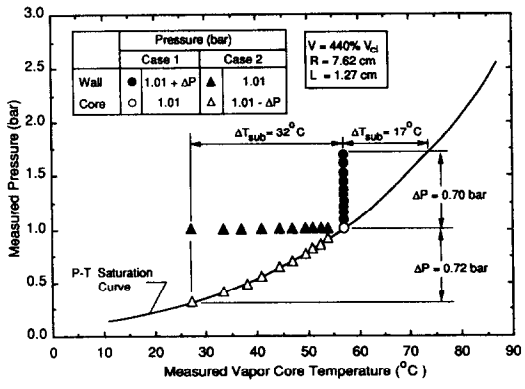

FIG. 7. Effect of pressure-induced subcooling due to rotating the liquid layer.

the marked increase in CHF manifested in Fig. 6. However, it should be emphasized that operating at a very low core pressure is not necessarily an effective means for enhancing CHF since saturated CHF decreases with decreasing pressure. It should also be noted that the enhancement of CHF due to subcooling becomes less significant for smaller layer thicknesses because of a smaller ΔP.

Centrifugal force effect

Vessels having two different radii were tested in the present study to isolate the effects of CHF enhancement due to stream-wise curvature and flow velocity. CHF measurements are plotted versus stirrer tip velocity in Fig. 8 for a fill volume equal to 100% V_{cl}. On the average a 36% increase in CHF was observed for the 4.19 cm radius vessel compared to the 7.62 cm radius vessel. This large enhancement could not be attributed to changes in subcooling since at most a 2.0°C subcooling was measured for the 100% V_{cl} fill volume.

In order to provide equal stirrer tip velocities, the stirrer in the 4.19 cm test vessel must rotate at almost twice the speed as in the 7.62 cm test vessel. Liquid layer agitation increases with increasing rotational speed (due to higher frequency of blade passes) and at first was believed to be a contributor to the observed CHF enhancement. Two different stirrer designs were tested to examine the influence of agitation. Surprisingly, no significant differences in CHF were measured between the two-bladed and the four-bladed stirrers, as shown in Fig. 8. Apparently, two blades produced a stream-wise velocity similar to that produced by four blades and the increased agitation generated by the additional blades was not effective in enhancing vapor removal from the boiling surface. CHF enhancement was, therefore, a result of the centrifugal force generated due to stream-wise curvature.

Figure 8 also displays a unique feature of the present system not found in most boiling systems: a lack of CHF dependence on heater length. This important observation will be discussed in the next section.

4. CHF CORRELATION

The experimental trends presented indicate that stream-wise curvature increases CHF by virtue of centrifugal force and subcooling of the liquid layer. An empirical CHF model will be constructed in this section which attempts to quantify these effects.

A characteristic velocity must first be developed that is representative for the flow conditions experienced in a stirred vessel. Velocity measurements were not made in the present study. However, limited information is available from other sources describing local velocity measurements in similar flow configurations.

Nagata [23] and Hiraoka *et al.* [24] showed that the stream-wise velocity in the liquid layer followed Rankine's combined vortex (i.e., solid body rotation away from the wall and a free vortex towards the test vessel wall). Nagata suggested that the velocity profile outside the thin wall boundary layer be modeled as

$$U = r\omega \qquad R - t < r < R_c \tag{1}$$

$$U = R_c\omega\left(\frac{R_c}{r}\right)^c \qquad R_c < r < R \tag{2}$$

with $c = 0.8$. At a distance $r = R_c$, the velocity profile in equation (1) changes from that of solid body rotation to a free vortex.

Pressure measurements were used to test the validity of equations (1) and (2). The momentum equation was integrated with respect to r assuming the axial and radial velocities are small compared to the stream-wise velocity, as verified by Nagata for the geometry of stirrer considered in the present study. The value

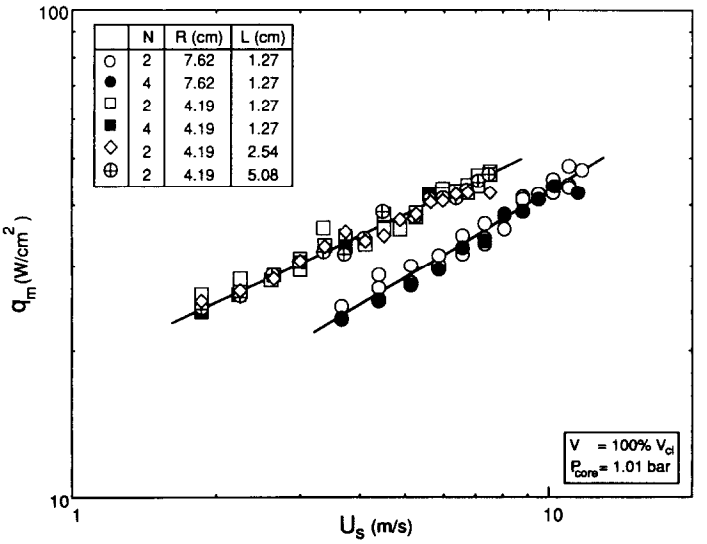

FIG. 8. Effects of radius curvature, number of stirrer blades and heater length on CHF.

of R_c used in equations (1) and (2) was fitted experimentally by matching the calculated pressures with the experimentally measured values. R_c was determined to be 92% of the stirrer radius which provided the best agreement between the measured and predicted pressures for all fill volumes and rotational speeds. Figure 9 shows that the calculated pressure, using the assumed velocity profile, compares well with the experimental data with an average deviation of 12% over the entire range of conditions of the present study.

The characteristic velocity used in correlating the present CHF data was selected as the velocity predicted from equation (2) at the vessel wall ($r = R$) because the wall boundary layer was thin for the high Reynolds numbers considered in the present study. The 'law of the wall' velocity profile proposed by Hiraoka *et al.* [24] for predicting velocity in the wall boundary layer of a stirred vessel was used to estimate the extent of this wall layer. At a rotational speed of 500 r.p.m., the stream-wise velocity was estimated to be 87% of the characteristic velocity, U_c, at a distance of only 50 μm from the vessel wall.

A technique proposed by Katto and Monde [25] was used to correlate the present CHF data for saturated conditions. This technique consists of expressing CHF as a function of five non-dimensional groups

$$\frac{q_{m,sat}}{\rho_g h_{fg} U_m} = C_1 \left(\frac{\rho_f}{\rho_g}\right)^{n_1} \left(\frac{\mu_g}{\mu_f}\right)^{n_2} \left(\frac{\sigma}{\rho_f U_m^2 L}\right)^{n_3} \times \left(\frac{\mu_f}{\rho_f U_m L}\right)^{n_4} \left(\frac{g(\rho_f - \rho_g)L}{\rho_f U_m^2}\right)^{n_5} \quad (3)$$

where $\sigma/(\rho_f U_m^2 L)$ is the inverse Weber number based on the heater length, L, and characteristic flow velocity, U_m.

Katto and Ishii [19] and Katto and Kurata [26] correlated CHF data according to equation (3) for a free surface jet and a submerged surface jet, respectively, for several different heater lengths. The second and fourth non-dimensional groups were not included since viscosity has little effect on CHF in most boiling systems. The fifth group was also excluded because the body force due to gravity was too weak to affect their flow conditions.

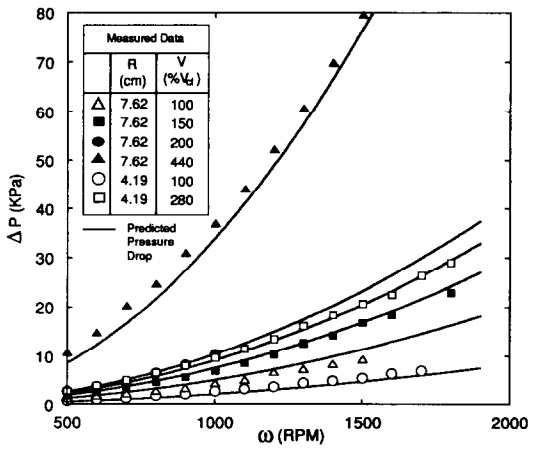

FIG. 9. Pressure rise across the liquid layer as a function of rotational speed and fill volume.

These free jet and submerged jet studies constitute linear flow reference conditions for the present system, one corresponding to a thin, and the other a thick liquid layer flowing over short heated surfaces. The fundamental difference between these two jet studies on one hand and the present study is the significance of the body force. The experimental correlations by Katto and Ishii and Katto and Kurata demonstrate how linear flow systems suffer a reduction in CHF with increasing heater length as liquid supply from the bulk flow to the boiling surface becomes increasingly restricted because of the increased vapor generation and accumulation downstream from the leading edge.

As indicated earlier, CHF in the present system was found to be independent of the heater length. Figure 10 is evidence that reducing the present CHF data with respect to the inverse Weber number based upon heater length precludes any agreement with linear flow correlations. Apparently, flow parallel to the curved heater surface must provide a mechanism for effective vapor removal which is independent of the heater length.

In order to correlate the present CHF data, it is important to identify an appropriate characteristic length for equation (3). Several length scales have been proposed in the past to reduce CHF data. The conditions leading to CHF were often linked to an instability between the liquid and vapor flow in the vicinity of the heater surface. For pool boiling at one-G conditions, Zuber *et al.* [7] postulated the Taylor instability as a necessary condition for CHF. They described the formation of vapor release jets perpendicular to the surface at sites separated by distances ranging between the Taylor unstable wavelength, $\lambda_{T,c}$, and the Taylor 'most dangerous wavelength', $\lambda_{T,d}$

$$2\pi\left(\frac{\sigma}{g(\rho_f - \rho_g)}\right)^{1/2} = \lambda_{T,c} \leqslant \lambda \leqslant \lambda_{T,d} = 2\pi\sqrt{3}\left(\frac{\sigma}{g(\rho_f - \rho_g)}\right)^{1/2}. \quad (4)$$

The former wavelength corresponds to the onset of instability of an *infinite* horizontal liquid–vapor interface with liquid residing above the vapor. Haramura and Katto [27] also used the unstable Taylor wavelength as a characteristic length scale in modeling pool boiling CHF from infinite horizontal surfaces.

Recently, Lee and Mudawar [28] modeled CHF in vertical subcooled flow in a vertical tube, postulating that bubbles near the wall coalesce into elongated bubbles having a characteristic length in the flow direction equal to the unstable Helmholtz wavelength. They constructed a CHF model pointing out dryout

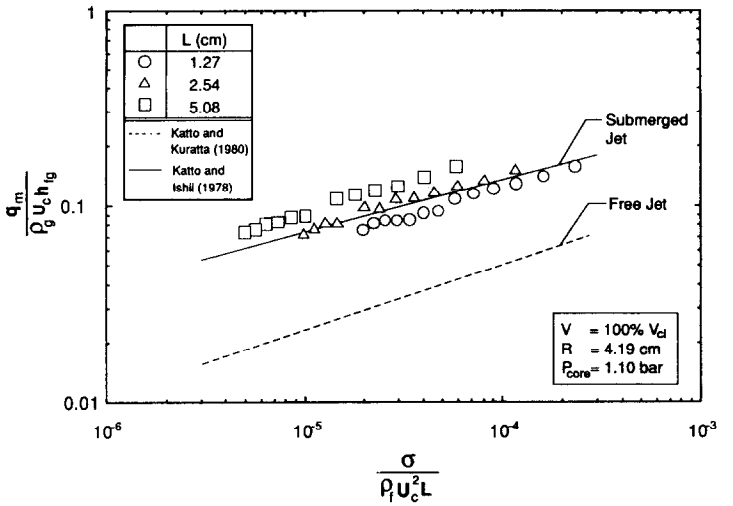

FIG. 10. Dimensionless CHF as a function of inverse Weber number based on heater length.

beneath the coalescent bubble as the precursor for CHF.

A characteristic length must be developed for the present geometry that incorporates the effects of centrifugal force and is independent of heater length. Significant insight into the proper choice of characteristic length, L, may be gained by investigating the hydrodynamic instabilities in a two-phase flow. In forced convection a vapor–liquid interface is created by coalescent bubbles leaving the heater surface. The interface becomes perturbed and grows as a result of the destabilizing inertial and body forces while surface tension helps to maintain interfacial stability for small wavelengths. When the wavelength of this disturbance exceeds a critical value, the interface becomes unstable.

An interfacial perturbation, z, can be assumed to follow the harmonic wave function

$$z = z_0 \cos\left\{\frac{2\pi}{\lambda}x\right\} \exp\left\{i\frac{2\pi}{\lambda}Ct\right\} \tag{5}$$

where z_0, λ, and C are, respectively, the perturbation amplitude at time $t = 0$, perturbation wavelength, and speed of propagation of the wave. Stability theory (see ref. [29]) for the configuration shown in Fig. 11 predicts that

$$\left(\frac{2\pi}{\lambda}\right)^2 C^2 = \frac{\sigma}{\rho_f+\rho_g}\left(\frac{2\pi}{\lambda}\right)^3 - \left(\frac{\rho_f-\rho_g}{\rho_f+\rho_g}\right)\left(\frac{2\pi}{\lambda}\right)a - \frac{\rho_f\rho_g}{(\rho_f+\rho_g)^2}\Delta U^2\left(\frac{2\pi}{\lambda}\right)^2 \tag{6}$$

where ΔU is the velocity difference between the two phases and a is the body force per unit volume perpendicular to the interface. The critical wavelength, λ_c, corresponds to the onset of instability and can be determined by setting $(2\pi/\lambda)C = 0$. The perturbation wavelength could assume values ranging from λ_c to λ_d, where λ_d is the wavelength associated with the fastest growth of instability; i.e., $d\{(2\pi/\lambda)/C\}\,d\lambda = 0$. Figure 11 shows that for low (especially sub-G) values of a, the instability becomes dominated by inertia, a condition well known as the Helmholtz instability (i.e. $\lambda_c = \lambda_{H,c}$ and $\lambda_d = \lambda_{H,d}$). For large body forces, on the other hand, the instability becomes fairly insensitive to inertia and may be predicted by the Taylor instability conditions given in equation (4). It can be concluded from Fig. 11 that (1) the range of centrifugal acceleration in the present study (5–150 G) is well above the range where inertial forces influence the instability, and (2) the corresponding values of λ_c and λ_d are much smaller than the smallest heater tested in the present study.

The bubble departure characteristics in the liquid layer were examined with the aid of both still photography, using a 35 mm camera equipped with a 20 μs flash, and video photography using a 6000 partial frames per second Kodak Ektapro 1000 motion analysis system. Viewing and lighting of the heater surface were both accomplished via a thin tubular boroscopic probe. The probe was inserted through the bottom window of the 7.62 cm test vessel in a direction parallel to the stirrer axis. Despite the relatively poor resolution of the photographic techniques used, due to a combination of the difficult lighting conditions within the vessel and fluid churning, some useful qualitative observations were possible at relatively low stirrer rotational speeds. At CHF, relatively large vapor bubbles were observed to coalesce and depart from the surface in a trajectory having a clear radial velocity component. The characteristic size of the coalescent bubbles decreased from approximately 6 mm at 0.5 G to 2 mm at 2.9 G. These values of coalescent bubble size are within 25% of the values of $\lambda_{T,c}$ predicted by equation (6).

It is interesting to note that when the Taylor wavelength, $\lambda_{T,c} = 2\pi[\sigma/\{(\rho_f-\rho_g)a\}]^{1/2}$, is used as the

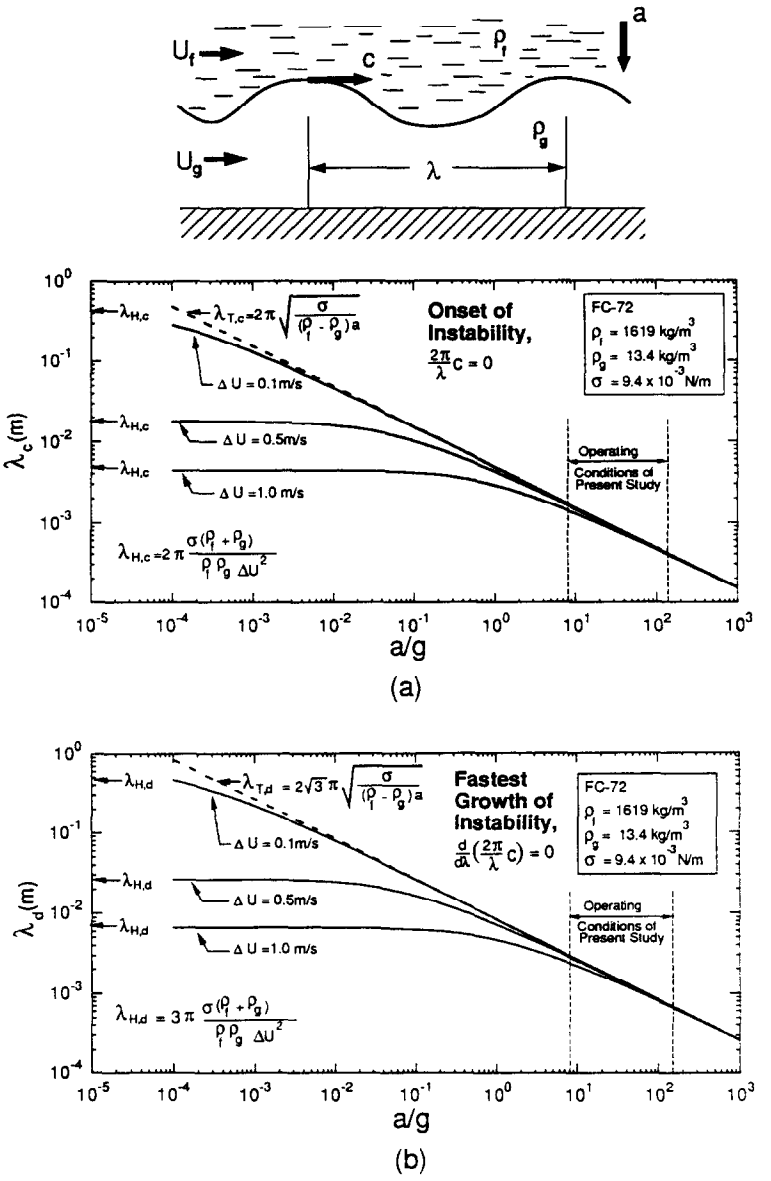

FIG. 11. Wavelength of interfacial perturbation corresponding to onset of instability (a) and fastest growth of instability (b).

characteristic length in equation (3) with $a = U_c^2/R$, both the third and fifth dimensionless groups become proportional to $[(\rho_f-\rho_g)\sigma/(\rho_f^2U_c^2R)]^{1/2}$.

Equation (3) must be modified to account for subcooling in the liquid layer. For every volume of vapor generated at the heater surface, an equal volume of subcooled liquid has to be brought to the saturation temperature before being evaporated. The ratio of subcooled to saturated CHF becomes

$$\frac{q_{m,sub}}{\rho_g h_{fg} U_c} = \frac{q_{m,sat}}{\rho_g h_{fg} U_c}\left(1+C_2\frac{\rho_f c_{pf}\Delta T_{sub}}{\rho_g h_{fg}}\right) \quad (7)$$

where $q_{m,sat}$ is given by equation (3) and C_2 must be less than unity. Neglecting the viscosity terms, the constants in equation (3), modified with the subcooling ratio given in equation (7), were determined by minimizing the absolute error between the correlation and experimental data. This resulted in the following correlations:

$$\frac{q_m}{\rho_g U_c h_{fg}} = 13.8\left(\frac{\rho_g}{\rho_f}\right)^{0.121}\left(\frac{(\rho_f-\rho_g)\sigma}{\rho_f^2U_c^2R}\right)^{0.408} \times\left(1+0.090\frac{\rho_f c_{pf}\Delta T_{sub}}{\rho_g h_{fg}}\right) \quad (8)$$

which has a mean absolute error of 6.8%, as shown in Fig. 12.

5. CONCLUSIONS

This paper examined the various geometrical parameters influencing CHF from a heater flush mounted

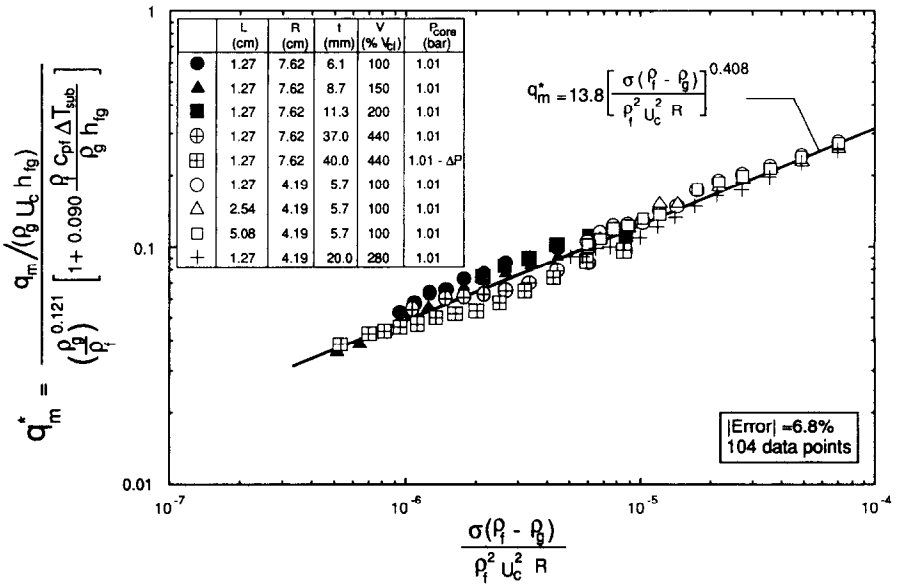

FIG. 12. Correlation of CHF data incorporating the effects of subcooling and centrifugal force.

on the inner wall of a cylindrical vessel cooled by a layer of dielectric liquid (FC-72) driven by a radial-bladed stirrer rotating about the axis of the vessel. Key findings from the study are as follows:

1. CHF was independent of the number of stirrer blades for a given rotational speed and vessel radius.
2. Unlike linear flow systems, the boiling performance and CHF in the rotating stirrer system were independent of heater length.
3. A unique aspect of the system performance was its CHF dependence on velocity and flow curvature. Equal velocities produced a higher CHF for the 4.19 cm vessel compared to the 7.62 cm vessel.
4. Greater fill volumes increased the pressure rise across the liquid layer and promoted a more stable liquid layer free interface.
5. A pressure rise across the liquid layer subcooled the liquid at the heater surface by as much as 32°C. Subcooling effects were more pronounced at lower core saturation pressures due to the increasing slope of the pressure–temperature saturation curve of the working fluid with increasing pressure.
6. An empirical CHF correlation was developed that accounts for the effects of the centrifugal force due to stream-wise curvature and subcooling due to the radial pressure gradient in the liquid layer.

Acknowledgements—Support for this work by the Purdue University Research Foundation is gratefully appreciated. The authors are also grateful to the 3M Company for donating FC-72 fluid for the study.

REFERENCES

1. A. Bar-Cohen, I. Mudawar and B. Whalen, Future challenges for electronic cooling. In *Research Needs in Electronic Cooling* (Edited by F. P. Incropera), pp. 70–77. National Science Foundation and Purdue University (1986).
2. R. E. Simons, Thermal management of electric packages, *Solid State Technol.* **26,** 131–137 (1983).
3. H. Merte and J. A. Clark, Pool boiling in an accelerated system, *ASME J. Heat Transfer* **83,** 233–242 (1961).
4. P. J. Marto and V. H. Gray, Effects of high acceleration and heat fluxes on nucleate boiling of water in an axisymmetric rotating boiler, NASA TN D-6307 (1971).
5. V. I. Usenko and S. N. Fainzil'berg, Effect of acceleration on the critical heat load with the boiling of Freons on elements having small transverse dimensions, *High Temperature* **12,** 490–495 (1974).
6. C. P. Costello and J. M. Adams, Burnout heat fluxes in pool boiling at high accelerations, *Proc. 2nd Int. Heat Transfer Conf.*, Boulder, CO, pp. 255–261 (1963).
7. N. Zuber, M. Tribus and J. W. Westwater, The hydrodynamic crisis in pool boiling of saturated and subcooled liquid, *Proc. 2nd Int. Heat Transfer Conf.*, Denver, CO, pp. 230–236 (1961).
8. C. P. Costello and W. E. Tuthill, Effects of acceleration on nucleate pool boiling, *Chem. Engng Prog. Symp. Ser.* **57,** 189–196 (1961).
9. W. A. Beckman and H. Merte, A photographic study of boiling in an accelerated system, *ASME J. Heat Transfer* **87,** 374–380 (1965).
10. A. Yerman, M. Becker, D. Kaminski and C. A. Neugebuer, In *Research Needs in Electronic Cooling* (Edited by F. P. Incropera), p. 83. National Science Foundation and Purdue University (1986).
11. J. R. Carver, C. R. Kakarala and J. S. Slotnik, Heat transfer in coiled tubes with two-phase flow, TID 20983, The Babcock and Wilcox Co. Research Center, Alliance, OH (1964).
12. Z. L. Miropol'skiy and V. Y. Pikus, Critical boiling heat fluxes in curved channels, *Heat Transfer—Sov. Res.* **1,** 74–79 (1969).
13. C. B. Gu, L. C. Chow and J. E. Beam, Flow boiling in a curved channel. In *Heat Transfer in High Energy/High Heat Flux Applications* (Edited by R. J. Goldstein, L. C. Chow and E. E. Anderson), ASME HTD Vol. 119, pp. 25–32 (1989).
14. W. R. Gambill and N. D. Green, Boiling burnout with water in vortex flow, *Chem. Engng Prog.* **54,** 93–102 (1958).

15. V. K. Dhir and J. H. Scott, On the superposition of injection induced swirl during enhancement of subcooled critical heat flux, *Int. J. Heat Mass Transfer* **30,** 2013–2022 (1987).
16. J. C. Collier, *Convective Boiling and Condensation*, 2nd Edn, p. 192. McGraw-Hill, New York (1972).
17. L. S. Tong, *Boiling Crisis and Critical Heat Flux*, p. 12. U.S. Atomic Energy Commission, National Technical Information Services (1972).
18. G. C. Vliet and G. Leppert, Critical heat flux for subcooled water flowing normal to a cylinder, *ASME J. Heat Transfer* **86,** 68–74 (1964).
19. Y. Katto and K. Ishii, Burnout in a high heat flux boiling system with a forced supply of liquid through a plane jet, *Proc. 6th Int. Heat Transfer Conf.*, Toronto, Canada, Vol. 1, pp. 435–440 (1978).
20. I. Mudawar, T. A. Incropera and F. P. Incropera, Boiling heat transfer and critical heat flux in liquid films falling on vertically-mounted heat sources, *Int. J. Heat Mass Transfer* **30,** 2083–2095 (1987).
21. I. Mudawar and D. E. Maddox, Critical heat flux in subcooled flow boiling of fluorocarbon liquid on a simulated electronic chip in a vertical rectangular channel, *Int. J. Heat Mass Transfer* **32,** 379–394 (1989).
22. J. E. Galloway and I. Mudawar, Boiling heat transfer from a simulated microelectronic heat source to a dielectric liquid film driven by a rotating stirrer, *ASME-HTD Heat Transfer in Electronics* **111,** 67–77 (1989).
23. S. Nagata, *Mixing and Applications*, pp. 126–131. John Wiley, New York (1975).
24. S. Hiraoka, R. Ito, I. Yamada, K. Sawada, M. Ishiguro and S. Kawamura, Law of the wall and velocity defect law in fully turbulent non-baffled agitated vessel, *J. Chem. Engng Japan* **8,** 156–161 (1975).
25. Y. Katto and M. Monde, Burnout in a high heat-flux boiling system with an impinging jet, *Int. J. Heat Mass Transfer* **21,** 295–305 (1978).
26. Y. Katto and C. Kurata, Critical heat flux of saturated convective boiling on uniformly heated plates, *Int. J. Multiphase Flow* **6,** 575–582 (1980).
27. Y. Haramura and Y. Katto, A new hydrodynamic model of critical heat flux applicable widely to both pool and forced convection boiling on submerged bodies in saturated liquids, *Int. J. Heat Mass Transfer* **26,** 389–399 (1983).
28. C. H. Lee and I. Mudawar, A mechanistic critical heat flux model for subcooled flow boiling based on local bulk flow conditions, *Int. J. Multiphase Flow* **14,** 711–728 (1988).
29. H. Lamb, *Hydrodynamics*, 6th Edn, p. 373. Dover, New York (1932).

ACCROISSEMENT DU FLUX CRITIQUE THERMIQUE PAR SOUS-REFROIDISSEMENT DE LIQUIDE ET FORCE CENTRIFUGE INDUITE PAR LA COURBURE DE L'ECOULEMENT

Résumé—Des expériences sont conduites pour établir la faisabilité du refroidissement de sources à haut flux, montées en affleurement dans la paroi interne d'un récipient cylindrique, par un liquide diélectrique qui s'écoule à grande vitesse parallèlement à la paroi. Le mouvement du fluide est induit par la rotation d'un agitateur ayant des pales radiales autour de l'axe du récipient. L'étude examine particulièrement l'accroissement du flux critique thermique (CHF) attribué au sous-refroidissement du liquide et à la force centrifuge induite par la rotation du fluide. Ceci implique l'utilisation de récipients de rayons différents, 4,19 et 7,62 cm, trois longeurs de chauffe 1,27, 2,54 et 5,08 cm, des agitateurs ayant deux ou quatre pales. Le CHF est indépendant de la longueur de chauffe et du nombre de pales. L'accroissement de CHF est amélioré en augmentant le volume de remplissage en liquide, la vitesse de rotation et/ou en diminuant le rayon de courbure. Le système facilite l'évacuation de la chaleur pour des conditions de parois isothermes sur un large domaine de flux thermique. Une formule de CHF est présentée qui tient compte des effets de sous-refroidissement et de force centrifuge pour toutes les conditions expérimentées.

ERHÖHUNG DER KRITISCHEN WÄRMESTROMDICHTE DURCH UNTERKÜHLUNG UND ERZEUGUNG VON ZENTRIFUGALKRÄFTEN DURCH STROMLINIENKRÜMMUNG

Zusammenfassung—Es wird die Anwendbarkeit eines Kühlverfahrens für sehr starke Wärmequellen experimentell untersucht. Die Wärmequellen sind an der Innenwand eines zylindrischen Behälters bündig angeordnet und werden mit hoher Geschwindigkeit von einer dielektrischen Flüssigkeit wandparallel überströmt. Die Strömung wird durch einen Rührer hervorgerufen, der in der Achse des zylindrischen Behälters angeordnet ist und radiale Schaufeln besitzt. Die Untersuchung konzentriert sich auf die Erhöhung der kritischen Wärmestromdichte durch Flüssigkeitsunterkühlung und durch die zentrifugalen Kräfte infolge der Flüssigkeitsrotation. Dazu werden Versuchsbehälter mit unterschiedlichen Innenradien (4,19 cm und 7,62 cm), 3 Heizflächenlängen (1,27 cm; 2,54 cm; 5,08 cm) sowie Rührer mit 2 und mit 4 Schaufeln verwendet. Die Ergebnisse zeigen, daß die kritische Wärmestromdichte von der Heizflächenlänge und der Anzahl der Rührerschaufeln unabhängig ist. Eine Erhöhung der kritischen Wärmestromdichte ergibt sich durch eine Erhöhung der eingefüllten Flüssigkeitsmenge sowie der Rotationsgeschwindigkeit und/oder einer Verringerung des Behälterradius. Die untersuchte Anordnung verbessert den Wärmeübergang bei nahezu isothermen Bedingungen an der Wand über einen weiten Bereich von Wärmestromdichten. Abschließend wird eine Korrelation für die kritische Wärmestromdichte vorgestellt, die den Einfluß der Unterkühlung und der Zentrifugalkräfte für alle untersuchten Bedingungen berücksichtigt.

УВЕЛИЧЕНИЕ КРИТИЧЕСКОГО ТЕПЛОВОГО ПОТОКА ЗА СЧЕТ НЕДОГРЕВА ЖИДКОСТИ И ЦЕНТРОБЕЖНОЙ СИЛЫ, ВЫЗВАННОЙ КРИВИЗНОЙ ТЕЧЕНИЯ

Аннотация—Экспериментально оценивается возможность охлаждения мощных тепловых источников, установленных вровень с внутренней стенкой цилиндрической емкости, за счет интенсивного течения диэлектрической жидкости, параллельного стенке емкости. Течение жидкости вызывалось вращением мешалки с радиальными лопастями вокруг оси емкости. Основное внимание уделялось изучению увеличения критического теплового потока (КТП), связанного с недогревом жидкости и центробежной силой, возникающей при вращении жидкости. В экспериментах использовались емкости с внутренними радиусами, составляющими 4,19 и 7,62 см, три различные длины нагревателя, равные 1,27; 2,54 и 5,08 см, а также двух- или четырехлопастные мешалки. Найдено, что КТП не зависит от длины нагревателя и количества лопастей мешалки. Возрастание КТП достигалось за счет увеличения объема жидкости, скорости вращения и (или) уменьшения радиуса кривизны. Используемая система способствовала теплоотводу при близких к изотермическим условиям на стенке в широком интервале изменений теплового потока. Предложено обобщающее соотношение для КТП, в котором учитываются эффекты недогрева и центробежной силы при всех экспериментальных условиях.